A Highly Active Star Decahedron Cu Nanocatalyst for Hydrocarbon Production at Low Overpotentials

*Chungseok Choi, Tao Cheng, Michelle Flores Espinosa, Huilong Fei, Xiangfeng Duan, William A. Goddard III, and Yu Huang**

The electrochemical carbon dioxide reduction reaction (CO$_2$RR) presents a viable approach to recycle CO$_2$ gas into low carbon fuels. Thus, the development of highly active catalysts at low overpotential is desired for this reaction. Herein, a high-yield synthesis of unique star decahedron Cu nanoparticles (SD-Cu NPs) electrocatalysts, displaying twin boundaries (TBs) and multiple stacking faults, which lead to low overpotentials for methane (CH$_4$) and high efficiency for ethylene (C$_2$H$_4$) production, is reported. Particularly, SD-Cu NPs show an onset potential for CH$_4$ production lower by 0.149 V than commercial Cu NPs. More impressively, SD-Cu NPs demonstrate a faradaic efficiency of 52.43% ± 2.72% for C$_2$H$_4$ production at −0.993 ± 0.0129 V. The results demonstrate that the surface stacking faults and twin defects increase CO binding energy, leading to the enhanced CO$_2$RR performance on SD-Cu NPs.

The ever-rising population and fossil fuel consumption present humanity with two major societal challenges: the brink of fossil fuel exhaustion and global climate change. A promising option to mitigate global warming and grant inexhaustible energy sources is to developing materials that efficiently catalyze greenhouse gas to value-added fuels and chemical feedstocks.[1–4] Starting with the pioneering electrochemical carbon dioxide reduction reaction (CO$_2$RR) in aqueous solutions by Hori et al.,[5] several other materials capable of reducing CO$_2$ have been identified.[6–8]

The most widely used CO$_2$RR catalysts to produce hydrocarbons including methane (CH$_4$) and ethylene (C$_2$H$_4$) are copper (Cu) based materials, which are the only catalysts shown to produce hydrocarbons (such as CH$_4$ and C$_2$H$_4$) with appreciable

reaction rates and efficiency.[9–11] At pH 6.8, electrochemical CO$_2$RR to CH$_4$ or C$_2$H$_4$ are thermodynamically favorable at 0.17 and 0.08 V versus reversible hydrogen electrode (RHE, referenced to all potentials).[9] However, in order to attain high specific activity and high faraday efficiency (FE) of CO$_2$RR, commercial Cu foils and NPs require high applied overpotentials (>1 V overpotential) due to the kinetically sluggish reaction pathways.[12] Unfortunately, such high applied potential also causes Cu electrochemical migration, dissolution, and redeposition that sinter the Cu NPs.[10,13]

Thus, developing Cu electrocatalysts for CO$_2$RR with high selectivity and current density at low overpotentials remains a grand challenge, stimulating great scientific endeavors. Numerous chemical modifications and nanostructuring approaches have led to improvements in product selectivity and catalytic activity.[3–5,7,12,14,15] Since the study showing a linear correlation between grain boundary (GB) density and CO$_2$RR performance by Li et al.,[16] GBs have been explored as highly active catalytic sites for both CO$_2$RR and carbon monoxide reduction, which promoted the production of CO and formic acid.[2,12] Promotion of C2 products on Cu GBs has been predicted by Cheng et al., although in Li's studies the production of ethylene is low.[17] Cheng et al. also reported a theoretical study showing that highly active twin boundaries (TBs) on the Au surface can be superior to GBs and other defects for CO$_2$RR.[18] Hence it would be interesting to realize Cu nanostructures with high TB for CO$_2$RR.

Multiple-twinned NPs such as icosahedron and star decahedron (SD) NPs are ideal structures to provide surface TBs, which have demonstrated enhanced performance in catalytic performance in various reactions.[19–25] Icosahedral and decahedral noble metal NPs (Ag, Au, Pt, and Pd) have been reported,[20–25] however, synthesis of multiple-twinned Cu NPs without rod structures has remained a challenge, due to the high reactivity and oxidation tendency of Cu.[20,26] TBs of Cu are more susceptible to oxidation than bulk Cu, leading to the etching of TB-rich NPs during the nucleation stage.[20,26] Another reason for the difficulty of creating Cu TB-rich NPs is the relatively high internal strain energy of Cu compared to Ag and Au because of the relatively high Young's modulus of Cu.[27,28]

Herein, we report the synthesis of fivefold twinned SD Cu nanoparticles (SD-Cu NPs) that show greatly enhanced

C. Choi, M. Flores Espinosa, Prof. Y. Huang
Department of Materials Science and Engineering
University of California, Los Angeles
Los Angeles, CA 90095, USA
E-mail: yhuang@seas.ucla.edu

Dr. T. Cheng, Prof. W. A. Goddard III
Materials and Process Simulation Center (MSC) and Joint Center for Artificial Photosynthesis (JCAP)
California Institute of Technology
Pasadena, CA 91125, USA

Dr. H. Fei, Prof. X. Duan
Department of Chemistry and Biochemistry
University of California, Los Angeles
Los Angeles, CA 90095, USA

**ADVANCED
SCIENCE NEWS**
www.advancedsciencenews.com

**ADVANCED
MATERIALS**
www.advmat.de

CO_2RR performance compared to commercial Cu NPs. Specifically, SD-Cu NPs showed 0.149 V lower onset potential for CH_4 production compared to commercial Cu NPs, as well as a high FE in the C_2H_4 production of 52.43% ± 2.72% at −0.993 ± 0.0129 V compared to 37.08 ± 6.87% at −1.009 ± 0.0113 V for commercial Cu NPs. Quantum mechanics (QM) calculations suggest that the surface TBs and multiple stacking faults on the surface of the SD-Cu NPs lead to the observed improvement.

In our experiments, to reduce the presence of oxygen in the solvent, we heated oleylamine (OAm) at 70 °C for 30 min. During colloid nucleation and growth, the twinned seeds are generally preferred at smaller sizes and transform into single crystal when they grow bigger. Hence slow growth rate and capping agent are typically used in order to arrest twinned nanostructures during the colloidal growth process.[20,29] To this end, we used a weak reduction agent (L-Ascorbic acid), a low (Cu(II) acetylacetonate) concentration, and low synthesis temperature (130 °C). When the reaction temperature was increased from 130 to 150 °C or 170 °C (Figure S1, Supporting Information), the twinned structures disappear, due to a higher growth rate that leads to bigger NP size and the transformation from the twinned structure to the polycrystalline structure (see the Supporting Information for details). The prepared SD-Cu NPs were characterized by transmission electron microscopy (TEM) and high-resolution TEM (HRTEM) (**Figure 1**) and powder X-ray diffraction (PXRD). The PXRD patterns of the colloidal products matched with that of the Cu JCPDS (#00-004-0836; Figure S2, Supporting Information). The average size of the Cu NPs was determined to be 30±1.89 nm, averaging over more than 100 particles (Figure 1a and Figure S3, Supporting Information). The HRTEM images show that Cu NPs exhibit a typical star shape with fivefold TBs crossing the edges of a decahedron (Figure 1b–d).[30] The measured angles between two adjacent TBs are 71.5 – 72.5°, matching those of SDs (Figure 1c,d). The structure of the Cu NPs was further analyzed by fast Fourier transform (FFT).[30] Within an SD-Cu NP, each TB was denoted OA, OB, OC, OD, and OE, respectively (Figure 1c,d). The FFTs of two typical SD-Cu NPs (Figure 1c,d) are shown in Figure 1e,f respectively. The FFTs show corresponding fivefold symmetry of {111} spots where A, B, C, D, and E are formed by each OA, OB, OC, OD, and OE TBs. Both HRTEM and FFT images matched well with that of fivefold twinned decahedron structure.[31,32] The complex splitting of FFT spots indicates the formation of bands of twin defects, and the elongation of spots in FFT images suggests steps on the SD-Cu NPs (Figure 1e,f).[31,32] We also applied inverse FFT at the Bragg spots (B, E) (Figure 1e) and (A, B, D, and E) (Figure 1f) on FFT images, to generate selectively filtered power spectrum on TBs.[33] The results confirm the bands of thin twin defects observed on HRTEM images (Figure 1g,h), and the inverse FFT TBs show well-matched angles (Figure 1g,h) with those in HRTEM (Figure 1c,d).

We studied the CO_2RR performance for these SD-Cu NPs with a gas-tight H cell by analyzing gas and liquid products at different applied potentials between −0.6 and −1.05 V in CO_2 saturated 0.1 M $KHCO_3$ (pH 6.8) at room temperature under atmospheric pressure. 0.01 mg Cu was loaded to the rotating disk electrode and measured by inductively coupled plasma atomic emission spectroscopy to evaluate the current density
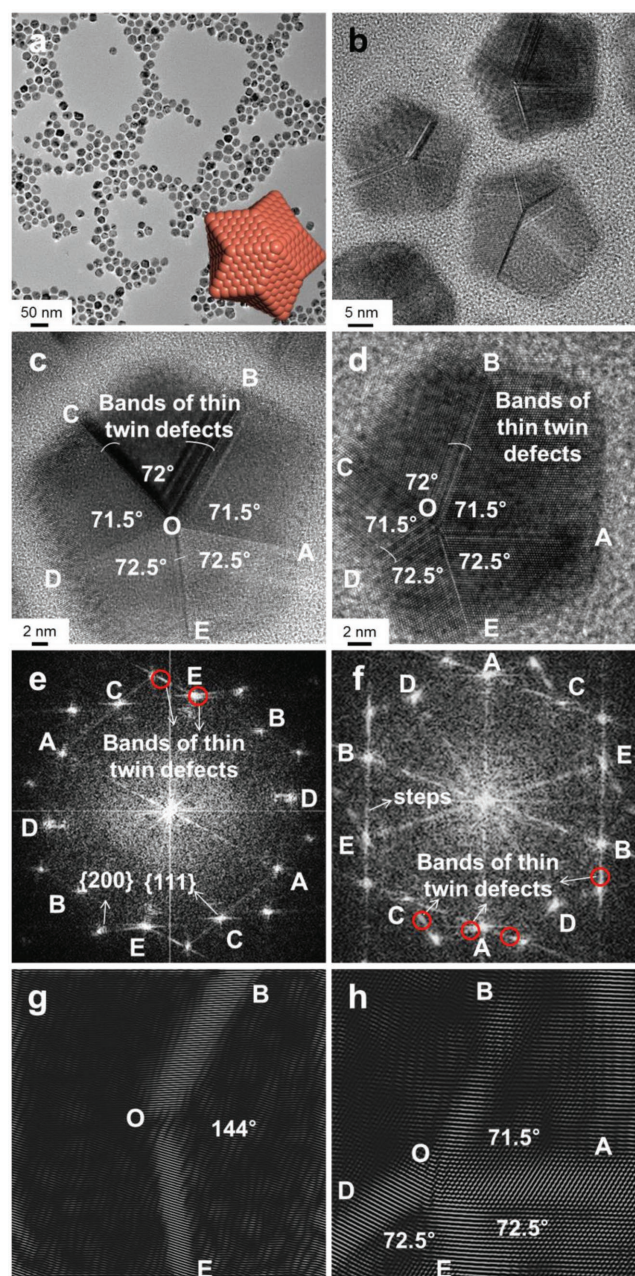

Figure 1. a) Low-magnification TEM image of SD-Cu NPs (inset is a schemed atomic structure), b) HRTEM image of SD-Cu NPs, c,d) fivefold twin symmetry on HRTEM images of SD-Cu NPs, e,f) fivefold twin symmetry on FFT images of SD-Cu NPs, g,h) inverse FFT of bands of thin twin defects on SD-Cu NPs.

and the electrochemically active surface area (ECSA; Figure S4 and S5, Supporting Information). Most products from these reactions were in the gas phase. Thus we focus our discussions of FE calculated by gas phase products (Tables S1 and S2, Supporting Information). In general, SD-Cu NPs showed better performance for CO_2RR than commercial Cu NPs. **Figure 2**a,b shows the FE of SD-Cu NPs and commercial Cu NPs, respectively. The major CO_2RR products from SD-Cu NPs were CH_4 and C_2H_4. Specifically, the formation of CH_4 started at −0.645 V

ADVANCED
SCIENCE NEWS
www.advancedsciencenews.com

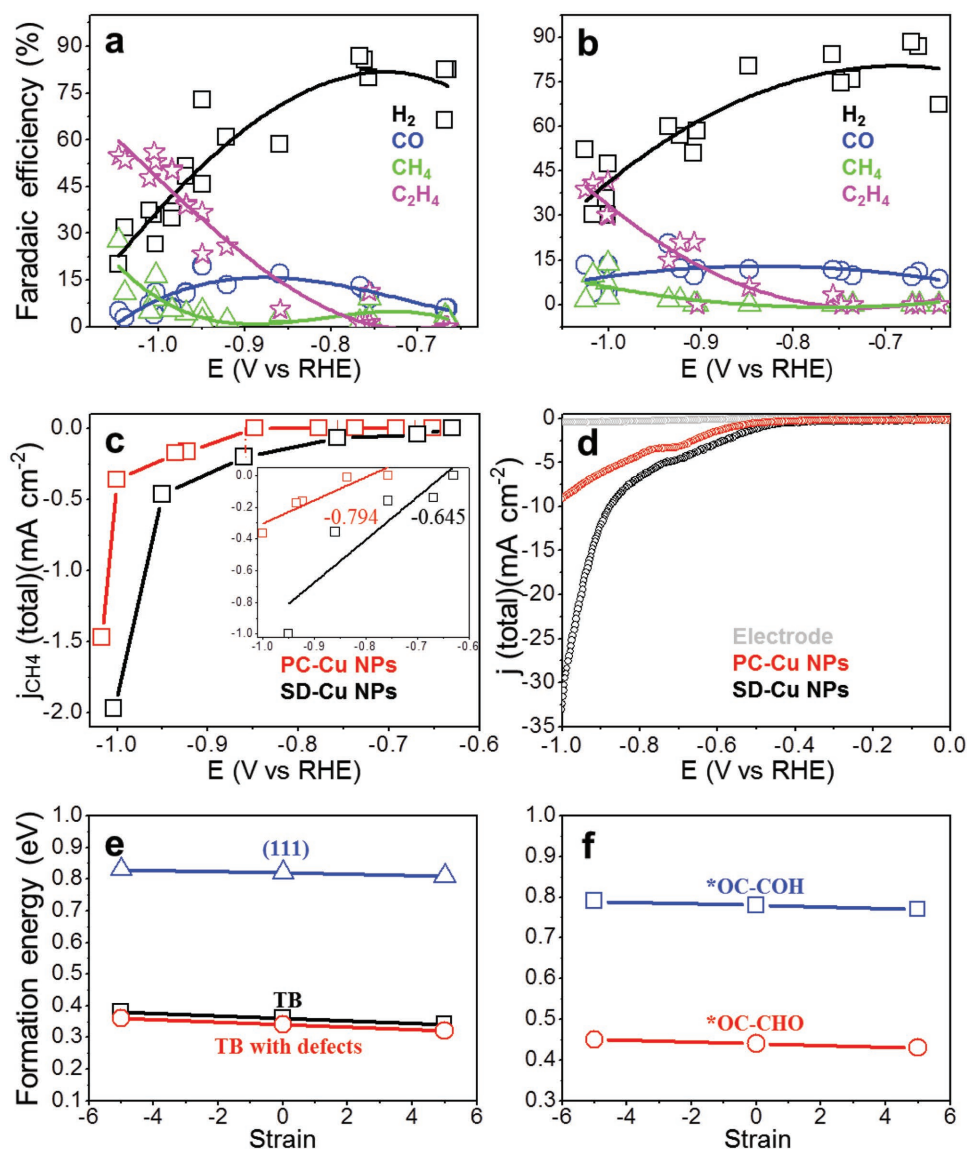**ADVANCED**
MATERIALS
www.advmat.de

Figure 2. a) FE of SD-Cu NPs, b) FE of PC-Cu NPs, c) ECSA normalized CH_4 partial current density, d) ECSA normalized total current density, e) the formation energy of *CHO on TB and TB with surface defects, and formation energy of *COH on Cu(111) as a function of surface strain, f) the formation energy of *OC—COH and *OC—CHO intermediates on TB as a function of surface strain.

(Figure 2a,c), and the FE of CH_4 remained below 10% up to −0.98 V (Figure 2a). At ≈−0.75 V, C_2H_4 formation initiated, with the FE escalating to 50.7% from −0.92 to −0.98 V (Figure 2a). The parallel production of C_2H_4 and CH_4 is similar to previously reported observations for a Cu foil.[6] In contrast, C_2H_4 was the primary CO_2RR product from commercial Cu NPs (Figure 2b), showing 20.90% and 40.92% C_2H_4 produced at −0.93 and −1.01 V (Figure 2b), consistent with the CO_2RR performance reported for commercial Cu NPs.[34] The polycrystalline structure of commercial Cu NPs (PC-Cu NPs) (Figure S6, Supporting Information) and the GBs may contribute to the observed difference in C_2H_4 production.[35]

Consistently, our SD-Cu NPs showed larger CH_4 partial current densities at all applied potentials than PC-Cu NPs (Figure 2c). Notably, the onset potential of CH_4 on SD-Cu NPs was only around −0.645 V, which is 0.149 V lower than that

of the PC-Cu NPs (−0.794 V) in Figure 2c. The onset potential for CH_4 was measured by using an interpolation method with linear fitting to initial CH_4 partial current density. The ECSA normalized current densities of SD-Cu NPs also exhibited higher current densities than PC-Cu NPs at all measured potentials (Figure 2d). In addition, the partial current density plot behavior for both C_2H_4 and CH_4 shows that SD-Cu NPs consistently exhibit a significantly higher intrinsic activity than PC-Cu NPs (Figure S7, Supporting Information).[36,37]

To understand the origin for the superior performance of SD-Cu NPs toward CO_2RR to CH_4, we carried out density functional theory (DFT) calculations using the level of Perdew–Burke–Ernzerhof functional (with Becke–Jonson damping D3 vdW correction) to investigate the critical reactive intermediates in the reaction pathway (see simulation details in Supporting Information). As found in our previous work, in the
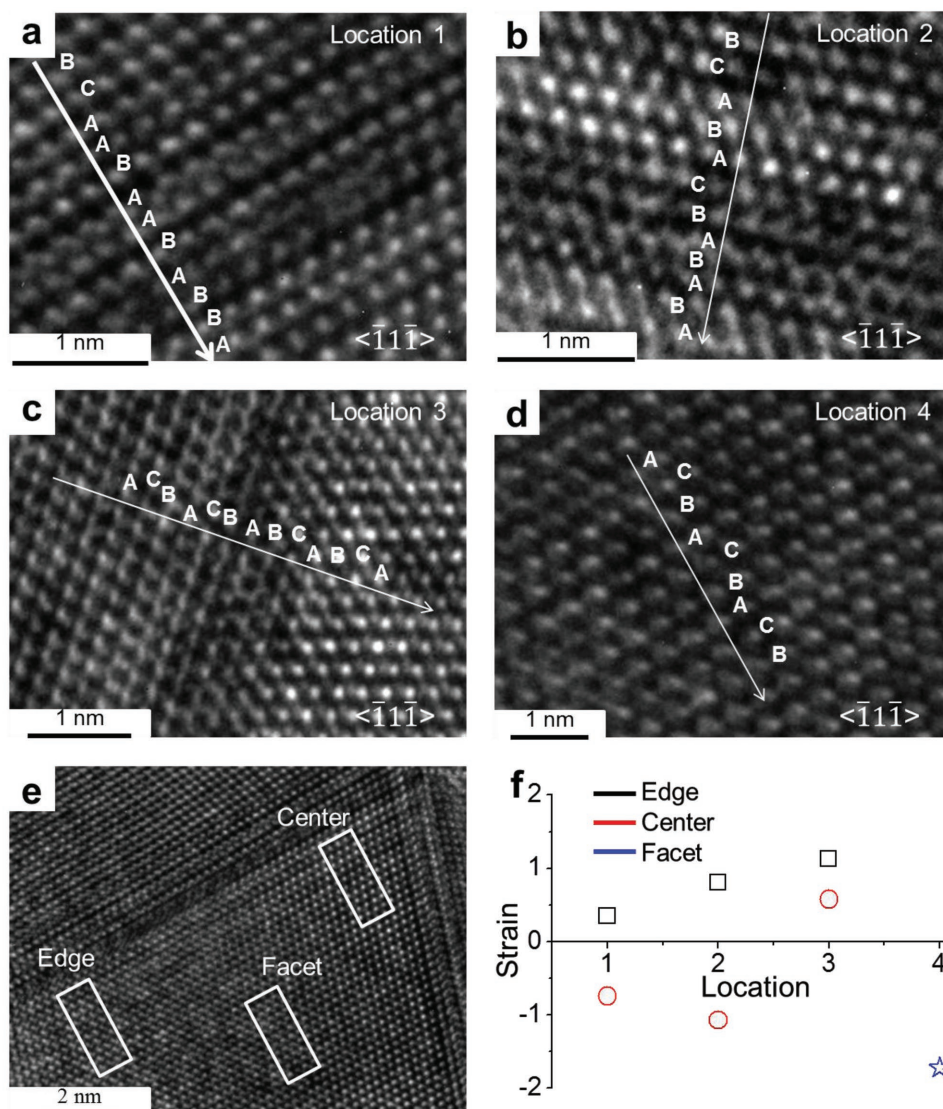
Figure 3. a–d) Four types of TB areas: a) parallel TB, b) TB with HCP stacking faults, c) single TB, d) center of (-11-1) facet. e) Strain analysis points: top, edge, and center. f) Strain measured at each above stacking.

reaction pathway for CH_4 formation via either *CHO formation or *COH formation, depending on the facet, determines the onset potential.[35,38] For the TB, we considered both possibilities in DFT calculations and found that the formation energy of *CHO is 0.36 eV which is considerable less than the formation energy of 0.89 eV for *COH. Thus, the DFT calculations predict that CH_4 formation on TBs is through *CHO. Furthermore, from nudged elastic band calculations, we calculated an energy barrier of 0.67 eV for formation of CH_4, which is 0.13 eV lower than the 0.80 eV energy barrier for the rate determining step of the CH_4 formation on Cu(111), obtained previously from the same level of DFT (Figure S8, Supporting Information).[38] This indicates an increase in the reaction rate. It is known that the (111) surface is a stable surface under the operando condition as confirmed by Kim et al.,[39] and that the (111) surface selectively reduces CO_2 to CH_4.[40] Accordingly, it is reasonable to consider that the (111) surface represents polycrystalline Cu despite the

presence of other minor sites (such as steps sites).[41] Figure 2e and Figure S8 in the Supporting Information show that compared with (111), the TB decreases both the reaction energy and the energy barrier of CH_4 formation, which explains the lower onset potential of CH_4 formation we observed.

Another feature of Figure 2a is the competition between CH_4 and C_2H_4 as the applied potential goes more negative (less than −0.75 V). To investigate the formation of C_2H_4 on TB, we carried out DFT calculations for the two possible steps that might become rate limiting: the formation of *OC−COH and the formation of *OC−CHO.[35] DFT calculations show that on the TB the formation energy of *OC−CHO is 0.44 eV while the formation energy of *OC−COH is 0.78 eV (Figure 2f). Thus, C_2H_4 formation through *OC−CHO is dramatically favored on the TB. This intermediate is formed from coupling of *CO and *CHO. Since *CHO is also an intermediates in CH_4 formation, we consider *CHO as the common intermediate for both

CH_4 and C_2H_4 formation (Figure S9, Supporting Information), which explains the experimental observations as follows: CH_4 likely dominates at low CO coverage, but C_2H_4 may dominate at high coverage.

At high overpotentials, however, the TB alone cannot explain the superior C_2H_4 production of SD-Cu NPs over most previously reported Cu based catalysts. It is well established that as multiple-twinned NPs grow larger, the internal strain on the surface increases.[31,32] Larger strain destabilizes multiple-twinned NPs, causing several stress release mechanisms on the surface of NPs to ameliorate the increasing internal stress. Interestingly, the stress-release mechanism induces grooving edges on multiple-twinned NPs and additional structural defects on such surfaces as steps and stacking faults.[31,32] Furthermore, the formation of the bands of thin twin layers in one of the {111} sections on the decahedrons could cause HCP stacking faults enclosing the parallel thin twin layers.[32,42] It has been estimated that Cu decahedrons NPs can maintain a balance between surface energy and strain energy in size that is less than ≈30 000 atoms (≈13 nm).[43] Indeed our 30 nm SD-Cu NPs, bands of TBs (Figure 1c–f), clearly exhibit rich stacking faults (**Figure 3**a–c) and small surface strain (Figure 3f) as a result of releasing of internal stress.

Three typical types of TBs in SD-Cu NPs are presented in Figure 3a–c: parallel TB, a TB with HCP stacking faults, and single TB. We determined the stacking sequence by assigning one layer as A and the subsequent layers as B, C, and so forth.[44] We analyzed the surface strain of SD-Cu NPs for these three types of TBs as well as at the (111) facet (Figure 3e,f). All measured strains near the edge of the SD-Cu NPs show tension strains while strains near the center of the SD-Cu show compression strains except for the case of a single TB (location 3), which is consistent with measured strains in the 2D projection TEM reported for gold decahedron NPs.[45,46] The single TB shows the highest tension strain (+1.128%) and the strains tend to decrease with bands of thin twin defects and with stacking faults, consistent with the stress release mechanism. Theoretical studies had predicted that only 1% surface strain could shift the d-band center of Pt by about 0.1 eV, which has a pronounced effect on the binding strength of reactive adsorbates.[47,48] Similarly, the relative high d-band center to the Fermi level in Cu NPs may lead to higher binding due to a lesser degree of occupancy of the antibonding states.[48]

Both, structure defects on catalyst surfaces (point, line, and planar defects) and applied tension strains, are known to shift upward the d-band center of surface atoms, which results in increased binding energy between the catalysts and the reacting molecules.[48] By using He I-ion ultraviolet (UV) source, valence-level electrons of Cu NPs were scanned from 0 to 16 eV, and the valence band spectra from each Cu NPs catalysts were measured by UV photoelectron spectroscopy (**Figure 4**a and Figure S10, Supporting Information).

We observed that SD-Cu NPs exhibit 0.2 eV higher d-band center than that of the PC-Cu NPs. The combined surface tension strains and generation of structural defects from stress releasing in SD-Cu NPs may contribute to the upshift of the d-band center that enhanced the binding of the catalyst surface to surface adsorbates.[48] Thus, a possible driving force of the increased C_2H_4 production observed in SD-Cu NPs may
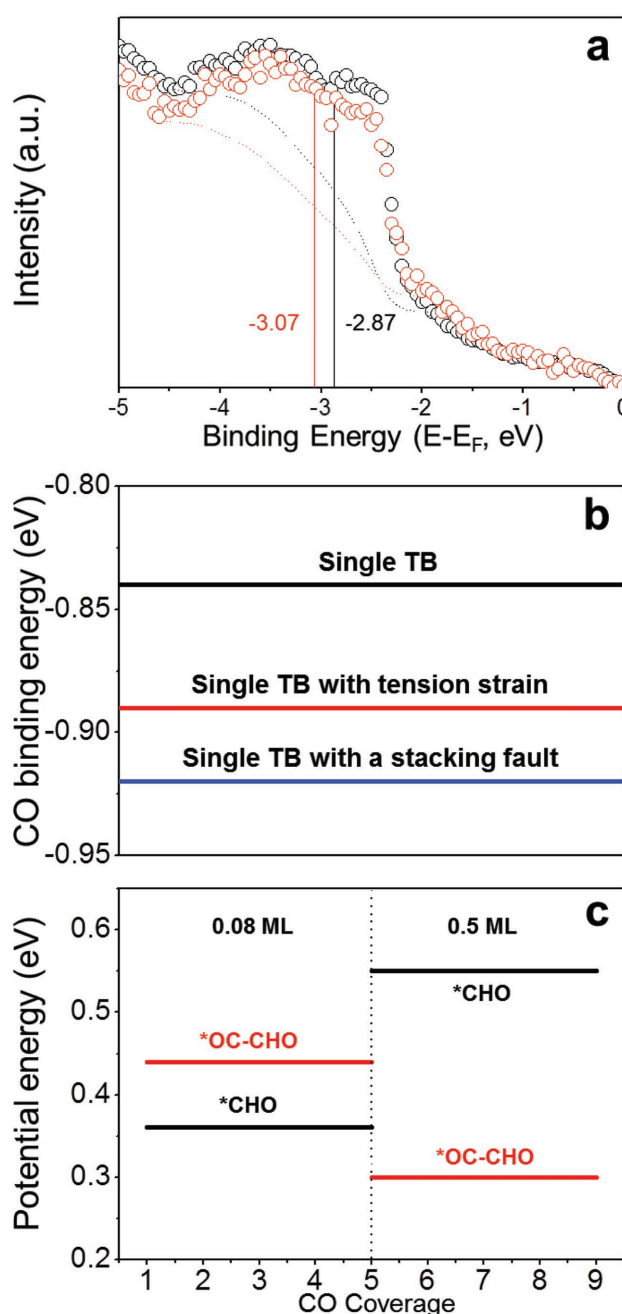

Figure 4. a) d-band center of SD-Cu NPs (black) and PC-Cu NPs (red), b) DFT energetics for various defect structures. Most stable is TB with a stacking fault, c) DFT relative energies for surface species. Low coverage favors CHO the intermediate for CH_4 production, and high coverage favors OC—CHO the intermediate for C_2H_4.

be the higher CO binding energy and increased CO coverage on the surface.[49]

DFT calculations were performed to elucidate these effects by constructing three types of TB atomic models; single TB, single TB with the tension strain, and single TB with the stacking fault. We found that a stacking defect with a single TB leads to a CO binding energy of −0.92 eV, which is about 0.08 eV stronger than single TB on Cu (111) surface (Figure 4b). We also found

that enrichment of CO concentration on Cu surface promotes C—C coupling to produce C_2H_4 (Figure 4c). For 0.5 monolayer, $\Delta E_{*OC-CHO}$ decreases to 0.30 eV, 0.14 eV lower than that in the dilute surface. However, ΔE_{*CHO} increases to 0.54 eV (Figure 4c). Because $\Delta E_{*OC-CHO}$ is lower than ΔE_{*CHO}, these QM calculations suggest that TB with higher CO concentration reduces CO_2 to C_2H_4 instead of CH_4, explaining the high FE of C_2H_4 and the suppression of CH_4 in SD-Cu NPs at higher potentials. In order to determine any structural changes induced by the CO_2RR, we analyzed the SD-Cu NPs after CO_2RR at −1 V for 1 h by using FFT, inverse FFT, and HRTEM (Figure S11, Supporting Information). Figure S11a in the Supporting Information illustrates no apparent change of SD-Cu NPs after 1 h of reaction. The bands of twin defects are still clear (Figure S11b, Supporting Information), which are marked clearly in the FFT, the inverse FFT images in Figure S11c,d are located in the Supporting Information.

To test the long-term operating ability of SD-Cu NPs, we performed the stability test under applied −1 V (RHE) for 12 h. We found that the FE_{C2H4} remained over 50% and the current remained 17 mA cm^{-2} up to 12 h, as shown in Figure S12 in the Supporting Information, confirming the high stability of the SD-Cu NPs with high FE_{C2H4} (over 50%). We also analyzed carefully structures of SD-Cu NPs after the 12 h stability test (Figure S13, Supporting Information). Compared to the 1 h reaction, we observed that SD-Cu NPs experienced some degree of aggregation, but individual SD-Cu NPs within the aggregate still maintained their morphology after 12 h. More importantly, TBs and bands of twin defect in SD-Cu NPs were clearly visible up to 12 h, and they remained apparent even in the aggregated SD-Cu NPs. (Figure S13b–g, Supporting Information) Thus, we attribute the long-term sustained activity of SD-Cu NPs (over 50% FE_{C2H4}) to the stability of the created TBs and bands of twin defects even during NP aggregation.

To summarize, we synthesized multiple-twined SD-Cu NPs with surface defects and tension strains. These SD-Cu NPs show an onset potential of −0.645 V, which is 0.149 V lower than for PC-Cu NPs. We found TBs on Cu NPs decrease the onset potential for CO_2RR to CH_4. Interestingly, we found that TBs combined with additional surface tension strain and stacking faults play essential roles in the increased FE for C_2H_4 formation and the suppression of CH_4 production. SD-Cu NPs show a dramatic improvement in C_2H_4 production in the potential range from −0.92 to −0.98 V with a concomitant decrease in CH_4 production by −0.98 V. Our DFT calculations show that the existence of TB significantly decreases the formation energy of *CHO, which facilies the formation of CH_4 at low overpotential. At high overpotential *CHO becomes a common intermediate for forming both CH_4 and C_2H_4, which explains the competition between CH_4 and C_2H_4.

Supporting Information

Supporting Information is available from the Wiley Online Library or from the author.

Acknowledgements

Conflict of Interest

The authors declare no conflict of interest.

Keywords

[1] J. L. DiMeglio, J. Rosenthal, *J. Am. Chem. Soc.* **2013**, *135*, 8798.
[2] C. W. Li, M. W. Kanan, *J. Am. Chem. Soc.* **2012**, *134*, 7231.
[3] Y. Chen, C. W. Li, M. W. Kanan, *J. Am. Chem. Soc.* **2012**, *134*, 19969.
[4] Y. Chen, M. W. Kanan, *J. Am. Chem. Soc.* **2012**, *134*, 1986.
[5] Y. Hori, K. Kikuchi, S. Suzuki, *Chem. Lett.* **1985**, *14*, 1695.
[6] Y. Hori, H. Wakebe, T. Tsukamoto, O. Koga, *Electrochim. Acta* **1994**, *39*, 1833.
[7] Y. Hori, *Modern Aspects of Electrochemistry*, Vol. *42*, Springer, New York **2008**, p. 89.
[8] H.-E. Lee, K. D. Yang, S. M. Yoon, H.-Y. Ahn, Y. Y. Lee, H. Chang, D. H. Jeong, Y.-S. Lee, M. Y. Kim, K. T. Nam, *ACS Nano* **2015**, *9*, 8384.
[9] K. P. Kuhl, E. R. Cave, D. N. Abram, T. F. Jaramillo, *Energy Environ. Sci.* **2012**, *5*, 7050.
[10] K. Manthiram, B. J. Beberwyck, A. P. Alivisatos, *J. Am. Chem. Soc.* **2014**, *136*, 13319.
[11] Y. Hori, R. Takahashi, Y. Yoshinami, A. Murata, *J. Phys. Chem. B* **1997**, *101*, 7075.
[12] X. Feng, K. Jiang, S. Fan, M. W. Kanan, *ACS Cent. Sci.* **2016**, *2*, 169.
[13] J. Huang, N. Hörmann, E. Oveisi, A. Loiudice, G. L. De Gregorio, O. Andreussi, N. Marzari, R. Buonsanti, *Nat. Commun.* **2018**, *9*, 3117.
[14] M. U. Khan, L. Wang, Z. Liu, Z. Gao, S. Wang, H. Li, W. Zhang, M. Wang, Z. Wang, C. Ma, J. Zeng, *Angew. Chem., Int. Ed.* **2016**, *55*, 9548.
[15] M. Asadi, K. Kim, C. Liu, A. V. Addepalli, P. Abbasi, P. Yasaei, P. Phillips, A. Behranginia, J. M. Cerrato, R. Haasch, P. Zapol, B. Kumar, R. F. Klie, J. Abiade, L. A. Curtiss, A. Salehi-Khojin, *Science* **2016**, *353*, 467.
[16] C. W. Li, J. Ciston, M. W. Kanan, *Nature* **2014**, *508*, 504.
[17] T. Cheng, H. Xiao, W. A. Goddard, *J. Am. Chem. Soc.* **2017**, *139*, 11642.
[18] T. Cheng, Y. Huang, H. Xiao, W. A. Goddard III, *J. Phys. Chem. Lett.* **2017**, *8*, 3317.
[19] L. Ruan, H. Ramezani-Dakhel, C. Lee, Y. Li, X. Duan, H. Heinz, Y. Huang, *ACS Nano* **2014**, *8*, 6934.
[20] J. Wu, L. Qi, H. You, A. Gross, J. Li, H. Yang, *J. Am. Chem. Soc.* **2012**, *134*, 11880.
[21] C. L. Johnson, E. Snoeck, M. Ezurdia, B. Rodriguez-González, I. Pastiriza-Santos, L. M. Liz-Marze, M. J. HŷTch, *Nat. Mater.* **2008**, *7*, 120.

[22] L. Ruan, C.-Y. Chiu, Y. Li, Y. Huang, *Nano Lett.* **2011**, *11*, 3040.

[23] H. Huang, H. Jia, Z. Liu, P. Gao, J. Zhao, Z. Luo, J. Yang, J. Zeng, *Angew. Chem.* **2017**, *129*, 3648.

[24] L. Ruan, E. Zhu, Y. Chen, Z. Lin, X. Huang, X. Duan, Y. Huang, *Angew. Chem.* **2013**, *125*, 12809.

[25] C. Wang, H. Yin, R. Chan, S. Peng, S. Dai, S. Sun, *Chem. Mater.* **2009**, *21*, 433.

[26] Y. Xia, Y. Xiong, B. Lim, S. E. Skrabalak, *Angew. Chem., Int. Ed.* **2009**, *48*, 60.

[27] B. Merle, Ph.D. thesis, Erlangen FAU Univ., Erlangen, Germany **2013**.

[28] H. Huang, F. Spaepen, *Acta Mater.* **2000**, *48*, 3261.

[29] Y. Ma, J. Zeng, W. Li, M. McKiernan, Z. Xie, Y. Xia, *Adv. Mater.* **2010**, *22*, 1930.

[30] A. F. D. Jong, W. Coene, D. V. Dyck, *Ultramicroscopy* **1989**, *27*, 53.

[31] M. J. Yacamán, J. A. Ascencio, H. B. Liu, J. Gardea-Torresdey, *J. Vac. Sci. Technol., B: Microelectron. Nanometer Struct.* **2001**, *19*, 1091.

[32] V. G. Gryazno, A. M. Kaprelo, A. E. Romano, I. A. Polonski, *Phys. Status Solidi B* **1991**, *167*, 441.

[33] Z. R. Dai, S. Sun, Z. L. Wang, *Surf. Sci.* **2002**, *505*, 325.

[34] C-T Dinh, T. Burdyny, M. G. Kibria, A. Seifitokaldani, C. M. Gabardo, F. P. D. Arquer, A. Kiani, J. P. Edwards, P. D. Luna, O. S. Bushuyev, C. Zou, R. Quintero-Bermudez, Y. Pang, D. Sinton, E. H. Sargent, *Science* **2018**, *360*, 783.

[35] T. Cheng, H. Xiao, W. A. Goddard III, *Proc. Natl. Acad. Sci. USA* **2017**, *114*, 1795.

[36] E. L. Clark, J. Resasco, A. Landers, J. Lin, L. T. Chung, A. Walton, C. Hahn, T. F. Jaramillo, A. T. Bell, *ACS Catal.* **2018**, *8*, 6560.

[37] M. R. Singh, E. L. Clark, A. T. Bell, *Phys. Chem. Chem. Phys.* **2015**, *17*, 18924.

[38] H. Xiao, T. Cheng, W. A. Goddard III, *J. Am. Chem. Soc.* **2016**, *138*, 483.

[39] Y.-G. Kim, A. Javier, J. H. Baricuatro, D. Torelli, K. D. Cummins, C. F. Tsang, J. C. Hemminger, M. P. Soriaga, *J. Electroanal. Chem.* **2017**, *793*, 113.

[40] K. J. P. Schouten, Z. Qin, E. P. Gallent, M. T. M. Koper, *J. Am. Chem. Soc.* **2012**, *134*, 9864.

[41] X. Liu, J. Xiao, H. Peng, X. Hong, K. Chan, J. K. Nørskov, *Nat. Commun.* **2017**, *8*, 15438.

[42] G. Lucadamo, D. L. Medlin, *Science* **2003**, *300*, 1272.

[43] F. Baletto, R. Ferrando, *Rev. Mod. Phys.* **2005**, *77*, 371.

[44] H. S. Nalwa, *Encyclopedia of Nanoscience and Nanotechnology* **2004**, *3*, 431.

[45] M. J. Walsh, K. Yoshida, A. Kuwabara, M. L. Pay, P. L. Gai, E. D. Boyes, *Nano Lett.* **2012**, *12*, 2027.

[46] B. Goris, J. D. Beenhouwer, A. D. Backer, D. Zanaga, K. J. Batenburg, A. Sánchez-Iglesias, L. M. Liz-Marzán, S. V. Aert, S. Bals, J. Sijbers, G. V. Tendeloo, *Nano Lett.* **2015**, *15*, 6996.

[47] P. Strasser, S. Koh, T. Anniyev, J. Greeley, K. More, C. Yu, Z. Liu, S. Kaya, D. Nordlund, H. Ogasawara, M. F. Toney, A. Nilsson, *Nat. Chem.* **2010**, *2*, 454.

[48] B. Hammer, J. K. Norskov, *Adv. Catal.* **2000**, *45*, 71.

[49] Y. Huang, A. D. Handoko, P. Hirunsit, B. S. Yeo, *ACS Catal.* **2017**, *7*, 1749.